Current-driven domain wall dynamics in ferrimagnets: micromagnetic approach and collective coordinates model

Eduardo Martínez[a], Víctor Raposo[a], Óscar Alejos[b,*]

[a] *Dpto. Física Aplicada, University of Salamanca, 37008 Salamanca, Spain*
[b] *Dpto. Electricidad y Electrónica, University of Valladolid, 47011 Valladolid, Spain*

Abstract

Theoretical studies dealing with current-driven domain wall dynamics in ferrimagnetic alloys and, by extension, other antiferromagnetically coupled systems as some multilayers, are here presented. The analysis has been made by means of micromagnetic simulations that consider these systems as constituted by two subsystems coupled in terms of an additional exchange interlacing them. Both subsystems differ in their respective gyromagnetic ratios and temperature dependence. Other interactions, as for example anisotropic exchange or spin-orbit torques, can be accounted for differently within each subsystem according to the physical structure. Micromagnetic simulations are also endorsed by means of a collective coordinates model which, in contrast with some previous approaches to these antiferromagnetically coupled systems, based on effective parameters, also considers them as formed by two coupled subsystems with experimentally definite parameters. Both simulations and the collective model reinforce the angular moment compensation argument as accountable for the linear increase with current of domain wall velocities in these alloys at a certain temperature or composition. Importantly, the proposed approach by means of two coupled subsystems permits to infer relevant results in the development of future experimental setups that are unattainable by means of effective models.

1. Introduction

The development of racetrack memories[1, 2] has attracted much interest in the recent times. Many efforts have been addressed in that way, particularly, the finding of optimal systems allowing fast displacement of domain walls (DWs) along them. Interfacial effects such as the Dzyaloshinskii-Moriya interaction, along with the generation of spin currents through the Spin-Hall effect (SHE)

*Corresponding author
Email addresses: edumartinez@usal.es (Eduardo Martínez), victor@usal.es (Víctor Raposo), oscar.alejos@uva.es (Óscar Alejos)

constituted a major step to this target.[3, 4, 5] The current-driven domain walls dynamics (CDDWD) in these systems are characterized by the absence of DW precessional regimes, against dynamics driven by magnetic fields or spin transfer torques.[6, 7] Nevertheless, the highest velocities reached by DWs under SHE are limited due to the reorientation of DW magnetic moments with the polarization of the spin current, so that velocity saturates as driving currents are increased.[8] Besides, experiments demonstrate that the DW transition type determines the velocity gained by DWs when tracking curved paths. In fact, some DWs can run faster or slower than others if they pass through a strip curved section. Velocities also differ from that gained by DWs tracking straight paths.[9]

Recent experimental evidence shows that current-driven DWs can reach velocities as fast as $1\text{km}\cdot\text{s}^{-1}$ along strips formed by antiferromagnetically coupled bilayers.[10] A dragging mechanism, resulting in a vanishing DW tilting, has been proved to allow such fast and synchronous tracking of DWs, even along curved paths. [10, 11] Besides, it has been found under certain conditions a linear relationship between DW velocities and current magnitudes, as also occurs in the case of certain ferrimagnetic alloys.[12]

Based on these promising experimental results, we provide full micromagnetic (μM) studies dealing with CDDWD in ferrimagnets (FiMs), also extendable to other antiferromagnetically coupled systems.[11] Our μM simulations treat them as constituted by two subsystems, in particular, two sublattices in FiMs, coupled by means of an additional intersystem exchange, and differing in their gyromagnetic ratios and saturation magnetization. Some other interactions can be accounted for in distinct manners within each subsystem, depending on the considered physical characteristics. μM simulations are also backed up with the help of an extended collective coordinates model in the form of a one-dimensional model (1DM).[11] In contrast with previous approaches to these systems, based on effective parameters,[13] this 1DM also considers systems as formed by two coupled subsystems with experimentally definite parameters. This is rather important, since the 1DM here presented does not require diverging parameters to match the results of the experimental evidence.[14] Importantly, the gyromagnetic ratio and the Gilbert damping parameter are taken as constants, contrarily to what it was suggested in the literature.[12] Realistic conditions can also be evaluated. Therefore, such approach permits to infer results not achievable from the mentioned effective models that can be of relevance in the development of future experimental setups. In particular, the work confirms the alignment of the magnetization with the direction of the electric current as responsible for the linear increase of DW terminal velocities with current. This alignment is remarkable when the angular moment compensation of sublattices occurs at a temperature close but not equal to the magnetization compensation temperature. Last but not least, the CDDWD along curved paths is found here to be dissimilar to that along straight ones, with distinct velocities depending on the DW type.

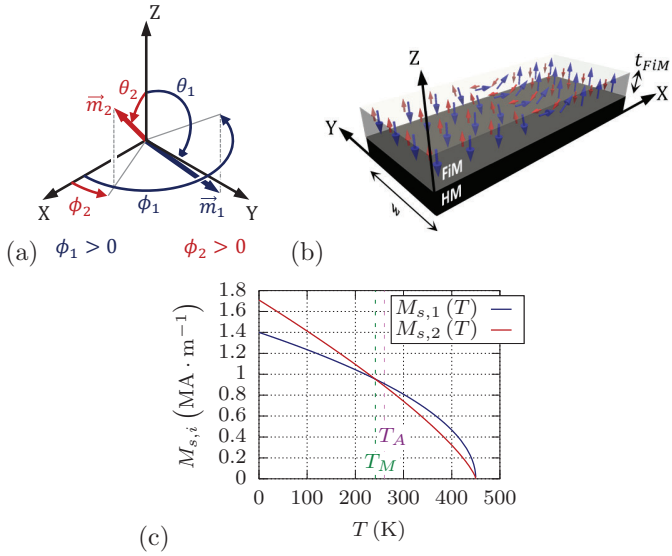

Figure 1: Two sublattices of respective magnetizations $M_{s,1}$ and $M_{s,2}$ constitute the ferrimagnetic strip: (a) unit vectors $\vec{m}_1$ and $\vec{m}_2$ defining the local orientation of the magnetization within each sublattice, (b) magnetic DW of Néel type amidst two domains oriented out of plane (the strip width w is here shown), and (c) temperature dependence of the magnetization of each sublattice.

2. Models

Figure 1 shows the main characteristics of the system under study. A FiM strip is deposited on top of a heavy metal (HM) layer. FiMs are considered to be formed by two sublattices of magnetizations $M_{s,1}$ and $M_{s,2}$ which are oriented along the unit vectors $\vec{m}_1$ and $\vec{m}_2$. Due to the perpendicular magnetic anisotropy, magnetizations point out of plane within the magnetic domains. Since magnetostatic interactions are much weaker than anisotropic exchange, such as the Dzyaloshinskii-Moriya interaction, DWs in the system are of Néel type. Temperature dependencies are also plotted in (c). Magnetizations decrease with temperature according to the law $M_{s,i}(T) = M^0_{s,i}\left(1 - \frac{T}{T_C}\right)^{a_i}$, $i = 1, 2$, $M^0_{s,i}$ being the respective magnetizations at zero temperature. T_C is the Curie temperature of the system, and a_i are some exponents depending on the sublattice components. Importantly, both magnetizations equalize at the magnetization compensation temperature T_M, leading to a null net magnetization, whereas magnetizations meet the condition $\frac{M_{s,1}}{\gamma_1} = \frac{M_{s,2}}{\gamma_2}$ at the angular momentum compensation temperature T_A, with γ_1 and γ_2 being the respective gyromagnetic ratios for each sublattice.

2.1. Micromagnetic modeling

In the framework of the μM model, the magnetization dynamics of a single ferromagnetic strip is described by the Landau-Lifshitz-Gilbert (LLG) equation.[15,

16] This idea can be generalized to study the magnetization dynamics in the FiM by considering two LLG equations, one for each sublattice, as:

$$\frac{d\vec{m}_i}{dt} = -\gamma_i \, \vec{m}_i \times \vec{H}_{eff,i} + \alpha_i \vec{m}_i \times \frac{d\vec{m}_i}{dt} + \\ + \vec{\tau}_{STT,i} + \vec{\tau}_{SOT,i}, \tag{1}$$

with $i = 1, 2$, and α_i being the respective Gilbert constants of each sublattice. The effective fields $\vec{H}_{eff,i}$ summarize all interactions within the system, including all intra-sublattice interactions together with an interaction term between both sublattices, i.e.:

$$\vec{H}_{eff,i} = \vec{H}_{ext} + \vec{H}_{dmg,i} + \vec{H}_{ani,i} + \vec{H}_{exch,i} + \vec{H}_{D,i}, \tag{2}$$

with $\vec{H}_{ext}$, $\vec{H}_{dmg,i}$, $\vec{H}_{ani,i}$, $\vec{H}_{exch,i}$ and $\vec{H}_{D,i}$ being respectively the external field, with components (H_x, H_y, H_z), the magnetostatic (demagnetizing) field, the anisotropy field, with out-of-plane and in-plane components given by the effective anisotropy constants $K_{eff,i}$ and $K_{sh,i}$, the isotropic exchange field and the anisotropic exchange field. The latter is responsible for the chiral nature of magnetic textures, and is determined by certain constants D_i. As for the isotropic exchange field, it can be reduced on first approach to a sum of the following terms:[17]

$$\vec{H}_{exch,i} = \frac{2A_i}{\mu_0 M_{s,i}} \nabla^2 \vec{m}_i + \frac{2A_{ij}}{\mu_0 M_{s,i}} \nabla^2 \vec{m}_j + \frac{B_{12}}{\mu_0 M_{s,i}} \vec{m}_j, \tag{3}$$

with $j = 1, 2$, and $j \neq i$. The first term here represents an intra-sublattice exchange field, given by the exchange stiffness A_i, and related to the local variation of the sublattice magnetization, whereas the latter is an inter-sublattice exchange field due to the misalignment of both sublattices, which is worked out from an energy density term in the form $\epsilon_{12} = -B_{12} \vec{m}_1 \cdot \vec{m}_2$, so that $B_{12} > 0$ (< 0) forces the antiparallel (parallel) alignment of the sublattices. The middle term in this exchange field stands for an additional inter-sublattice exchange due to the local variations of the magnetization in one of the sublattices. This term has been implemented into our homemade μM code.[11] However, no relevant differences in the case here presented have been found between the results either including or ignoring such an additional term. Finally, $\vec{\tau}_{STT,i}$ and $\vec{\tau}_{SOT,i}$ stand for the torques due to spin polarized currents, i.e., the spin transfer torques[15] and the spin-orbit torques[16], respectively. The former terms consist of adiabatic interactions $\vec{\tau}_{A,i}$, defined by certain values u_i, and their non-adiabatic counterparts $\vec{\tau}_{NA,i}$, related to these by the factors β_i, so that:

$$\vec{\tau}_{STT,i} = \vec{\tau}_{A,i} + \vec{\tau}_{NA,i} = \\ = u_i \left(\vec{u}_J \nabla\right) \vec{m}_i - \beta_i u_i \vec{m}_i \times \left(\vec{u}_J \nabla\right) \vec{m}_i, \tag{4}$$

where $\vec{u}_J$ represents the direction of the current density. The latter terms can be split into field-like torques with effective fields $H_{FL,i}$, and Slonczewskii-like

torques with effective fields $H_{SL,i}$, both to be further on defined. In fact,

$$\begin{aligned}\vec{\tau}_{SOT,i} &= \vec{\tau}_{FL,i} + \vec{\tau}_{SL,i} = \\ &= -\gamma_i H_{FL,i}\vec{m}_i \times \sigma - \gamma_i H_{SL,i}\vec{m}_i \times (\vec{m}_i \times \sigma)\,,\end{aligned} \tag{5}$$

where $\vec{\sigma}$ is the unit vector along the direction of the polarization of the spin current generated by SHE in the HM, that is, $\vec{\sigma} = \vec{u}_J \times \vec{u}_z$, since $\vec{u}_z$ defines the HM/FiM interface. $\vec{\sigma} = -\vec{u}_y$ for a longitudinal current so that $\vec{u}_J = \vec{u}_x$.[15, 18, 19]

2.2. Collective coordinates model

Starting from (1), and with the use of variational principles, a 1DM can be derived, leading to a set of equations that involve the instantaneous position q of a DW in the system and orientations ψ_i of the in-plane components of the magnetization of each sublattice with respect to the longitudinal axis of the strip. A note must be made at this time. The model could have considered different positions q_1 and q_2 for the magnetic transitions in each subnet. However, both a brief energetic argument and the study by means of micromagnetic simulations, allows inferring that the transitions occupy identical positions, i.e., $q = q_1 = q_2$. Thus, the ansatz $\theta_i = 2\arctan \mathrm{e}^{Q_i \frac{x-q}{\Delta}}$ and $\phi_i = \psi_i$ is to be used, θ_i and ϕ_i defining the local orientation of the magnetization in each sublattice, as shown in FIG.1(a), and Δ standing for the DW width. $Q_i = \pm 1$ indicates up-down $(+1)$ or down-up (-1) DW configurations within each sublattice. $Q_1 = -Q_2$ for antiparallel coupling of sublattices.

The derivation of the 1DM results in the following set of expressions (more details in Appendix A):

$$\begin{aligned}\alpha_1 \frac{M_{s,1}}{\gamma_1}\frac{\dot{q}}{\Delta} + \alpha_2 \frac{M_{s,2}}{\gamma_2}\frac{\dot{q}}{\Delta} + \frac{M_{s,1}}{\gamma_1}Q_1\dot{\psi}_1 + \frac{M_{s,2}}{\gamma_2}Q_2\dot{\psi}_2 = \\ = Q_1 M_{s,1}\left[H_z - \frac{\pi}{2}H_{SL,1}\cos\psi_1\right] + \\ + Q_2 M_{s,2}\left[H_z - \frac{\pi}{2}H_{SL,2}\cos\psi_2\right] + \\ + \frac{M_{s,1}}{\gamma_1}\beta_1\frac{u_1}{\Delta} + \frac{M_{s,2}}{\gamma_2}\beta_2\frac{u_2}{\Delta},\end{aligned} \tag{6a}$$

$$\begin{aligned}-Q_1\frac{\dot{q}}{\Delta} + \alpha_1\dot{\psi}_1 = -Q_1\frac{u_1}{\Delta} - \gamma_1\frac{H_{k,1}}{2}\sin(2\psi_1) + \\ + \gamma_1\frac{\pi}{2}Q_i H_{D,1}\sin\psi_1 - \gamma_1\frac{\pi}{2}H_{FL,1}\cos\psi_1 + \\ + \gamma_1\frac{\pi}{2}(H_y\cos\psi_1 - H_x\sin\psi_1) + \\ + \gamma_1\frac{2B_{12}}{\mu_0 M_{s,1}}\sin(\psi_1 - \psi_2),\end{aligned} \tag{6b}$$

$$
\begin{aligned}
-Q_2\frac{\dot{q}}{\Delta}+\alpha_2\dot{\psi}_2 = &-Q_2\frac{u_2}{\Delta}-\gamma_2\frac{H_{k,2}}{2}\sin\left(2\psi_2\right)+\\
&+\gamma_2\frac{\pi}{2}Q_2H_{D,2}\sin\psi_2-\gamma_2\frac{\pi}{2}H_{FL,2}\cos\psi_2+\\
&+\gamma_2\frac{\pi}{2}\left(H_y\cos\psi_2-H_x\sin\psi_2\right)+\\
&+\gamma_2\frac{2B_{12}}{\mu_0M_{s,2}}\sin\left(\psi_2-\psi_1\right),
\end{aligned}
\tag{6c}
$$

To ease notation, some values have been used in these equations, such as $H_{D,i}=\frac{D_i}{\mu_0 M_{s,i}\Delta}$, and $H_{k,i}=\frac{2K_{sh,i}}{\mu_0 M_s}$. The Sloncewskii-like term defined by means of the value $H_{SL,i}$ is related to the longitudinal current density J_{HM} along the HM layer through $H_{SL,i}=\frac{\hbar\theta_{SH,i}J_{HM}}{2|e|\mu_0 M_{s,i}t_{FiM}}$, with $\hbar$ being the reduced Plank constant, $|e|$ the absolute electron charge, $\theta_{SH,i}$ the spin-Hall angle for each sublattice and t_{FiM} the thickness of the FiM.[20] The field-like counterpart of this term can be regarded as proportional to it in a factor k_i, that is, $H_{FL,i}=k_iH_{SL,i}$.

3. Results

The CDDWD results here presented have been computed by means of μM simulations with the mentioned homemade code,[11] and the 1DM above developed. A common set of material parameters found in the literature[12] has been considered for the two sublattices ($i=1,2$): $A_i=70\frac{\mathrm{pJ}}{\mathrm{m}}$, $K_{eff,i}\approx K_{u,i}=1.4\frac{\mathrm{MJ}}{\mathrm{m}^3}$, $K_{u,i}$ being the magnetic uniaxial anisotropy constant of the FiM sublattices, $K_{sh,i}\approx 0$, $\alpha_i=0.02$, $D_i=0.12\frac{\mathrm{mJ}}{\mathrm{m}^2}$, $\theta_{SH,i}=0.155$, $k_i\approx 0$ and $u_i\approx 0$. The antiferromagnetic coupling between the two sublattices is accounted for by the parameter $B_{12}=-90\frac{\mathrm{MJ}}{\mathrm{m}^3}$.[17] The gyromagnetic ratios ($\gamma_i=\frac{g_i\mu_B}{\hbar}$, μ_B being Bohr's magneton) are different due to distinct Landé factors: $g_1=2.05$ and $g_2=2.0$. The temperature dependence of the magnetization of each sublattice is determined by the Curie temperature $T_C=450$K of the FiM, and $M^0_{s,1}=1.4\frac{\mathrm{MA}}{\mathrm{m}}$ and $M^0_{s,2}=1.71\frac{\mathrm{MA}}{\mathrm{m}}$, with $a_1=0.5$ and $a_2=0.76$. According to these values, the temperature of magnetization compensation is $T_M\approx 241.5$K, and the angular momentum compensation temperature is $T_A=260$K. The dimensions of the FiM strips are $w\times t_{FiM}=256\mathrm{nm}\times 6\mathrm{nm}$. With these parameters, DW width is $\Delta\approx 6$nm.

The computation of μM calculations requires a previous space discretization that, in our case, has been chosen to be as small as 1nm cell-size.

3.1. Transient response of domain walls in ferrimagnets

As a first result, the transient response of a DW in a FiM straight strip under the effect of a pulse of longitudinal current J_{HM} of a certain duration is presented in FIG.2. Graphs describe the DW displacement q and the DW orientation angles ψ_1 and ψ_2 computed at four different temperatures, including magnetization compensation and angular momentum compensation temperatures ($T\approx 240K$ and $T\approx 260K$, respectively). There is a good agreement

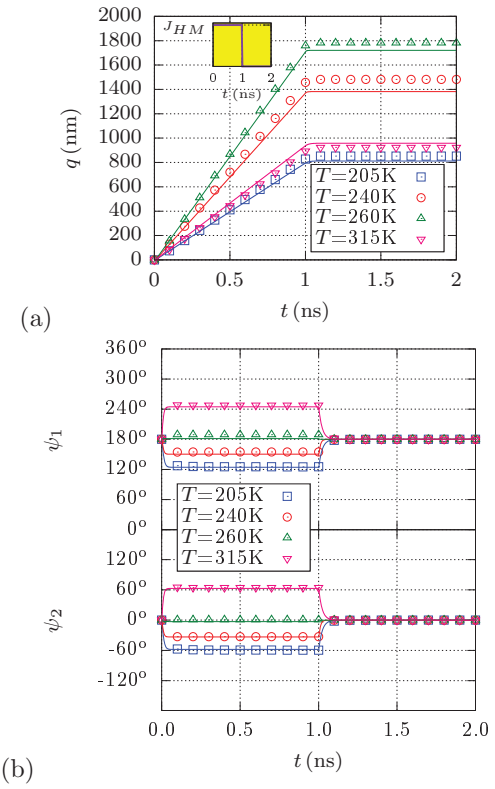

Figure 2: Transient response of a DW under the effect of a current pulse. Pulse amplitude and duration are $J_{HM} = 2\frac{\mathrm{TA}}{\mathrm{m}^2}$ and $t_p = 1$ns. The response is obtained at four different temperatures for a) DW position q, and b) DW magnetization angles of both sublattices ψ_1, and ψ_2. Dots correspond to μM simulations, while continuous lines are the results drawn by the 1DM.

between μM and 1DM results. Both methods reveal a fast response of DWs, whose terminal velocity can be then estimated as the quotient of DW run distance and pulse duration. Importantly, the low damping considered in these simulations, as recently suggested by some authors, [14] does not result in large domain wall inertia,[21, 22] quite the contrary.

It is to note that the highest velocity is reached at the angular momentum compensation temperature ($T \approx 260K$). At this temperature, a noticeable alignment between the DW moments of both sublattices and the longitudinal current occurs (DW magnetization angles are closer to either 0º and 180º than at other temperatures), with a rather slight misalignment between sublattices.

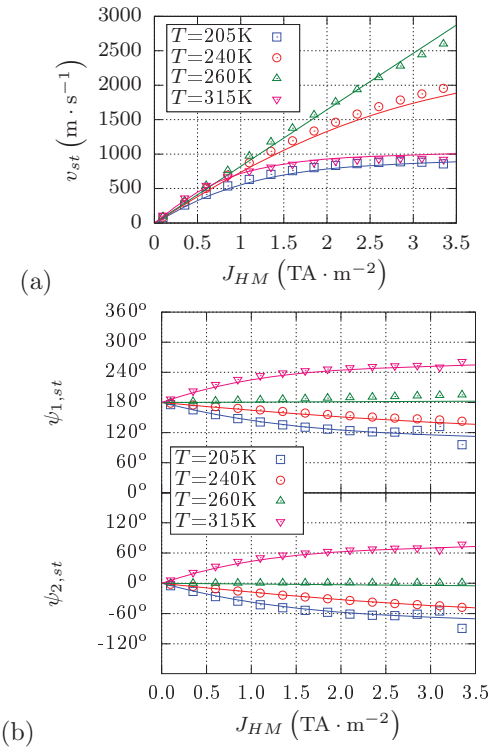

Figure 3: Dependence on current density J_{HM} of (a) DW terminal velocity v_{st}, and (b) DW stationary angles $\psi_{1,st}$ and $\psi_{2,st}$. Dots correspond to μM simulations, while continuous lines are the results drawn by the 1DM.

3.2. Stationary response of domain walls in ferrimagnets

3.2.1. Temperature dependence of CDDWD

FIG.3 shows the dependencies of DW terminal velocities, $v_{st} = \dot{q}_{st}$, and stationary DW angles $\psi_{1,st}$, and $\psi_{2,st}$ with J_{HM}, both micromagnetically computed (dots) and calculated using the 1DM (continuous lines). Curves are obtained for different temperatures. A relevant agreement of these results and experiments[12] has been found for currents above the experimental threshold values (the effect of some imperfections in realistic samples is to be discussed further on). The rather good agreement between μM and 1DM results is also noticeable. At the compensation temperature T_A, v_{st} increases almost linearly with current. Although the spin-polarized current promotes a slight misalignment between the magnetization of the sublattices, the linearity holds as long as sublattice internal DW moments remain closely oriented with the longitudinal direction, i.e., perpendicular to the spins of the spin-Hall current, as it can be checked also in FIG.3(b). Accordingly, a linear relationship between v_{st} and J_{HM} can be derived by considering DW angles completely oriented with the

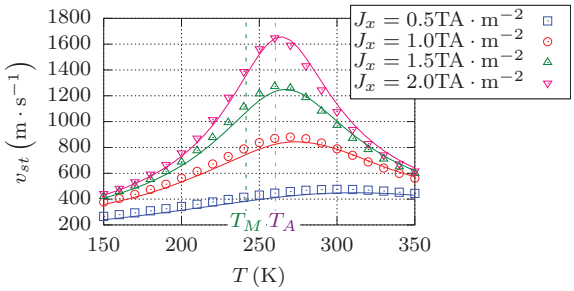

Figure 4: Dependence of the terminal velocity v_{st} with temperature for different driving currents obtained from μM simulations (dots), and the 1DM (continuous lines).

current direction:

$$v_{st} = \gamma_0 \frac{\Delta}{\alpha} \frac{\pi}{2} \frac{\hbar \theta_{SH} J_{HM}}{2\,|e|\,\mu_0 t_{FiM}} \frac{g_1 g_2}{(g_2 M_{s,1} + g_1 M_{s,2})}. \tag{7}$$

The general dependence of v_{st} on temperature for different driving currents is plotted in FIG.4. Low currents (blue curve) are not sufficient to disorientate sublattice magnetizations, so that v_{st} slightly varies in the considered temperature range. However, a peak around T_A is observable for high currents, when the spin-Hall induced torque tends to vanish and, consequently, the spin-Hall effective field, proportional to the longitudinal internal DW moment,[3, 19, 15] is optimized.

3.2.2. CDDWD dependence on external in-plane fields

- Longitudinal fields.

  In order to confirm the relevance of the alignment of DW moments with current, an additional study of the effects of in-plane fields on the CDDWD has been performed. First, results for a current density of $J_{HM} = 2\frac{\mathrm{TA}}{\mathrm{m^2}}$ and longitudinal fields B_x ranging from -300mT to $+300$mT are plotted in the graphs of FIG.5. These results confirm that the highest speed is reached when the DW moments of both sublattices are oriented with the current direction, and this occurs when the field and the net magnetization of the system are equally oriented. In fact, since the net magnetization in the system here analyzed has opposite orientation at $315K$ and $205K$, v_{st} decreases/increases with positive/negative fields (net magnetization and applied field are antiparallel/parallel) for the highest temperature and increases/decreases for the lowest one. In any case, the magnetization of each sublattice remains approximately antiparallel to each other in the whole range under study.

- Transverse fields.

  So as to promote the misalignment between sublattices, a transverse in-plane field B_y can be applied. FIG.6 present the corresponding results,

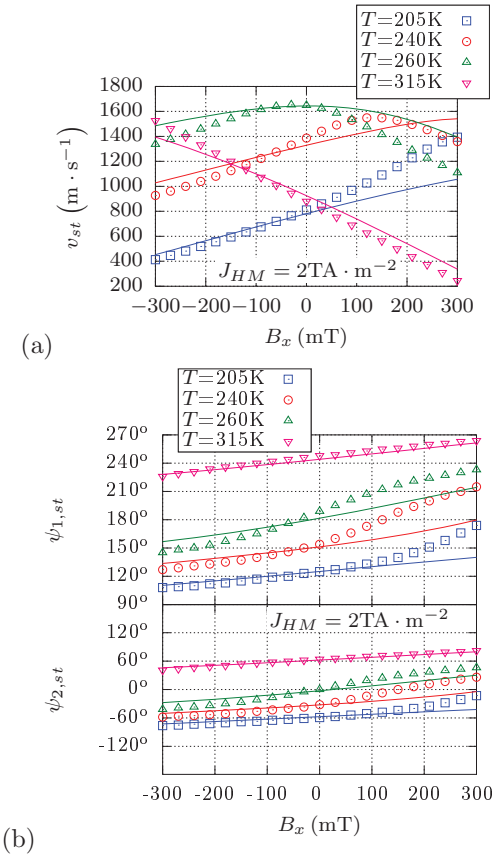

Figure 5: Dependence on longitudinal applied field B_x of (a) DW terminal speed v_{st}, and (b) DW stationary angles $\psi_{1,st}$ and $\psi_{2,st}$. A current density of $J_{HM} = 2\frac{\mathrm{TA}}{\mathrm{m}^2}$ has been used. As in other graphs, dots correspond to μM simulations, while continuous lines are the results drawn by the 1DM.

where DW terminal velocities and stationary values of the DW angles are plotted as a function of the longitudinal current J_{HM} with the transverse field as a parameter. The field and the polarization $\vec{\sigma}$ of the spin current now share the same direction. For both analyzed temperatures, an almost linear behavior is reached when both the field and $\vec{\sigma}$ are equally oriented, differently to the case when both vectors are antiparallel, and the linear behavior correspond to the cases when the DW moments of both lattices remain close to the longitudinal direction. In the absence of driving currents, the transverse in-plane field is not able to induce a continuous displacement of DWs, and a null v_{st} is obtained.

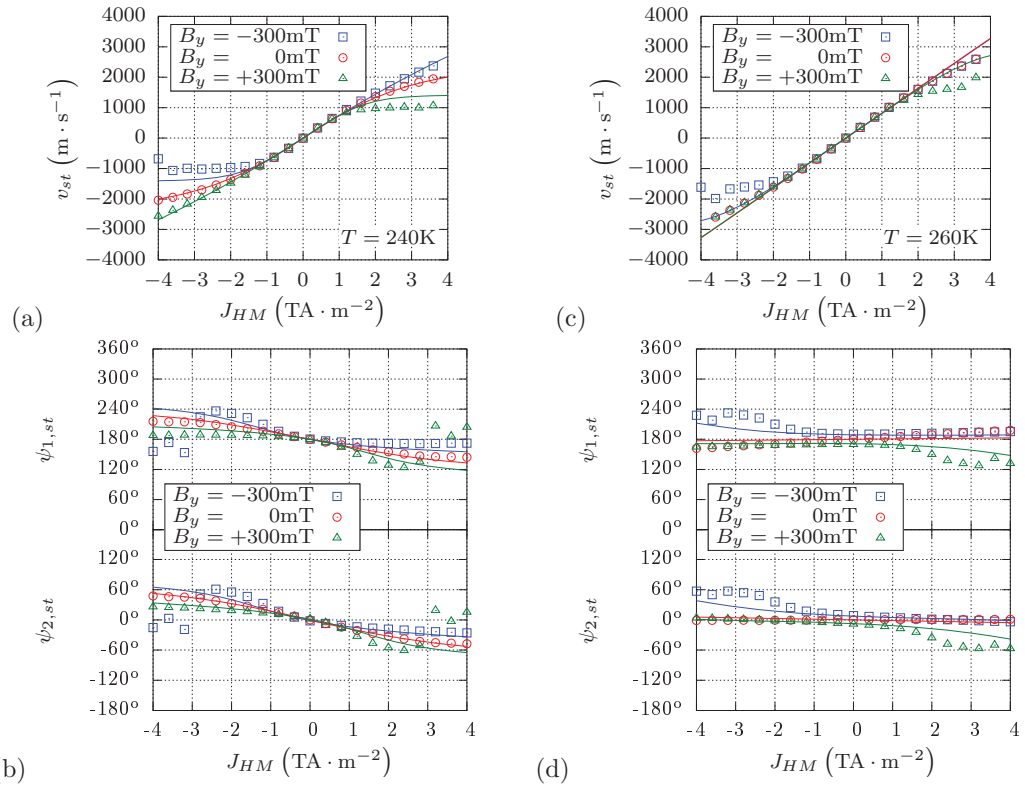

Figure 6: Dependence on current density J_{HM} with the transverse applied field B_y as a parameter of (a) DW terminal velocities v_{st} at $T = 240$K, (b) DW stationary angles $\psi_{1,st}$ and $\psi_{2,st}$ at $T = 240$K, (c) DW terminal velocities v_{st} at $T = 260$K, and (d) DW stationary angles $\psi_{1,st}$ and $\psi_{2,st}$ at $T = 260$K. Again, dots correspond to μM simulations, while continuous lines are the results drawn by the 1DM.

3.3. Realistic samples

The effect of imperfections on the CDDWD can also be included in our analysis. A certain granularity is added to the system to mimic these imperfections. Grains of 10nm-size have been used, characterized by an arbitrary orientation of their anisotropy axis around the out-of-plane direction. Two cases are here presented, either 5% or 10% variation of this orientation. Five distinct realizations have been performed for each granularity to obtain some statistically relevant results. An increasing threshold current with the degree of imperfections arise in this system (see FIG.7). The 1DM is also able to describe the CDDWD by using an additional periodic potential[20] of a certain amplitude and period equal to twice the grain size. The potential amplitude used in the case of 10% variation doubles that used in the 5% case.

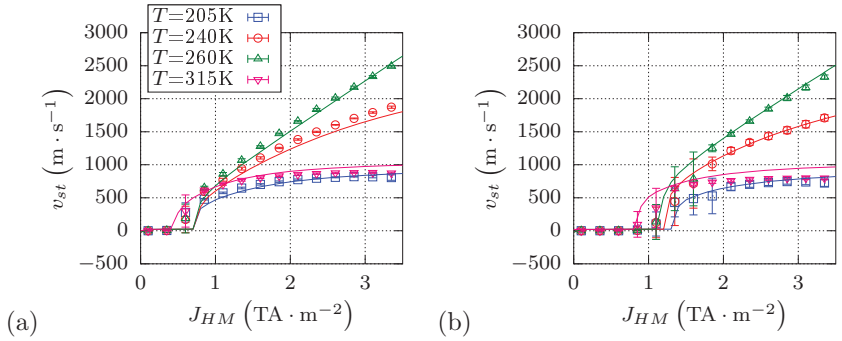

Figure 7: Emergence of a threshold current for strips with imperfections: (a) 5% anisotropy variation, and (b) 10% anisotropy variation. Dots correspond to μM simulations and continuous lines to the 1DM.

3.4. Application to the CDDWD along curved paths

Finally, we have also performed a μM analysis of the CDDWD along a strip with straight and curved parts at the most efficient case, i.e., $T = T_A$. Identical HM/FiM cross section has been adopted. Transient μM snapshots are shown in FIG.8. In the curved parts, the internal radius (r_i) is equal to the FiM strip width (w), i.e., $r_i = w = 256$nm. In the straight parts, DWs are very efficiently driven by the current injected along the HM without tilting. However, DWs tilt as they go through the curved parts, with similar tilting angles for all DWs of the two sublattices. We have verified that such a tilting is due to the non-uniform distribution of the current along the HM due to its curved shape. Importantly, the relative distance between adjacent DWs is not preserved after passing through the first curve. Therefore, these observations indicate the DW motion is sensitive to the curvature of the HM/FiM stacks, and further investigations are needed to correct this drawback for DW recording devices based on these systems.

4. Conclusions

μM simulations and the 1DM model have been proved to adequately describe the CDDWD in FiMs. In contrast with previous approaches, the procedure here presented is not based on phenomenological but on experimentally determined system parameters. This effective approach permits us, for example, to confirm that the basis of the linearity between terminal velocities and current densities at $T = T_A$ in FiMs is the fact that internal DW moments of the sublattices keep oriented along the longitudinal direction. Such a conclusion can be drawn because magnetic sublattices are separately considered and linked by means of an inter-lattice exchange. Not all of its capabilities have been here developed, since, for example, the parameters used for both sublattices are common and only differ in their respective saturation magnetizations and gyromagnetic ratios. Other differences have been already suggested in the literature, such as

Gilbert damping,[23, 18] or the effect of spin-orbit torques,[24, 25] which can also be covered by our models and could be essential to describe further experimental observations. Indeed, our approach permits to analyze the application of very distinct stimuli acting differently on the sublattices, such as spin transfer torques, both adiabatic and non-adiabatic, the mentioned spin-orbit torques or in-plane magnetic fields. The effects of imperfections and geometry have indeed been addressed. Our models are not only applicable to FiMs deposited on HMs, but to any system that can be described by means of two interlaced subsystems. In fact, due to its versatility, our models can serve as a cornerstone of future experiments regarding CDDWD, which can be of relevance in the development of FiM based devices.

Acknowledgments

The authors want to thank Dr. Luis Sánchez-Tejerina for his valuable comments, and also acknowledge the support by project MAT2017-87072-C4-1-P from the Spanish government, and project SA299P18 from the Junta de Castilla y León.

Appendix A. Development of the collective coordinates model (1DM)

The LLG equation (1) also admits a resolution with the help of variational principles, then requiring the description of the magnetization textures by means of some collective coordinates as the instantaneous position q of a DW in the system, and the orientations ψ_i of the in-plane components of the DW moments of each sublattice with respect to the longitudinal axis of the strip. These coordinates determine the local orientation of the magnetization through the well-known ansatz $\theta_i = 2\arctan \mathrm{e}^{Q_i \frac{x-q}{\Delta}}$ and $\phi_i = \psi_i$, θ_i and ϕ_i defining the local orientation of the magnetization in each sublattice, Δ accounting for the DW width, and Q_i determining the magnetization transition, as they have been defined in the main text. Previous to the application of the ansatz, system energies can be expressed as:

$$\epsilon_{exch,i} = A_i \left(\nabla \vec{m}_i\right)^2 = A_i \left[\left(\nabla\theta_i\right)^2 + \sin^2\theta_i \left(\nabla\phi_i\right)^2\right], \tag{A.1a}$$

$$\epsilon_{ani,i} = K_{u,i}\left[1 - \left(\vec{m}\cdot\vec{u}_k\right)^2\right] = K_{u,i}\sin^2\theta_i, \tag{A.1b}$$

$$\epsilon_{dmg,i} = -\frac{1}{2}\mu_0 M_{s,i}\vec{H}_{dmg}\cdot\vec{m}_i = \left(K_{dmg,i} + K_{sh,i}\sin^2\phi_i\right)\sin^2\theta_i, \tag{A.1c}$$

$$\begin{aligned}\epsilon_{ext,i} &= -\mu_0 M_{s,i}\vec{H}_{ext}\cdot\vec{m}_i = \\ &= -\mu_0 M_{s,i}\left(H_x\sin\theta_i\cos\phi_i + H_y\sin\theta_i\sin\phi_i + H_z\cos\theta_i\right),\end{aligned} \tag{A.1d}$$

$$\begin{aligned}\epsilon_{DM,i} &= D_i\left[m_{z,i}\left(\nabla\vec{m}_i\right) - \left(\vec{m}_i\cdot\nabla\right)m_{z,i}\right] = \\ &= D_i\left[\cos\phi_i\frac{\partial\theta_i}{\partial x} + \sin\phi_i\frac{\partial\theta_i}{\partial y} + \sin\theta_i\cos\theta_i\left(\sin\phi_i\frac{\partial\phi_i}{\partial x} - \cos\phi_i\frac{\partial\phi_i}{\partial y}\right)\right],\end{aligned} \tag{A.1e}$$

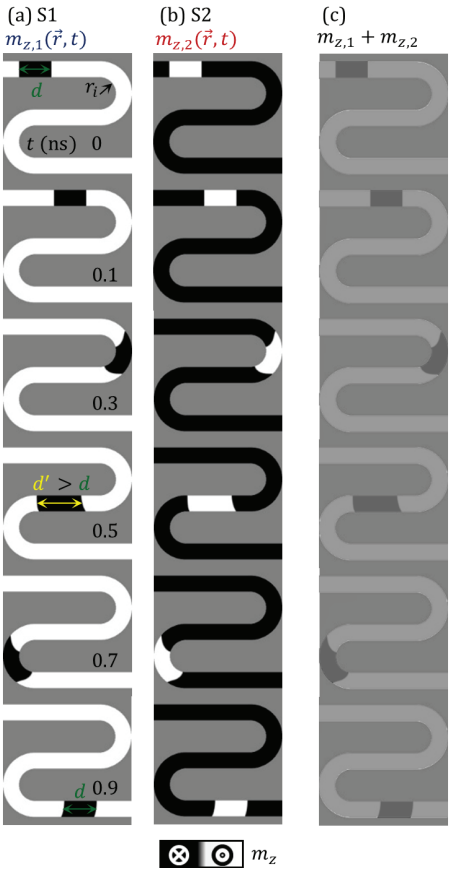

Figure 8: μM snapshots of the CDDWD of two adjacent DWs along curved paths. The current density in the straight paths, where it is uniform, is of $J_{HM} = 1.5\frac{\mathrm{TA}}{\mathrm{m}^2}$, and the temperature chosen is $T = T_A$. The panels represent: a) out of plane component $m_{z,1}$ of the magnetization along the first sublattice, b) out of plane component $m_{z,2}$ of the magnetization along the second sublattice, c) out of plane component of the net magnetization $m_{z,1} + m_{z,2}$ along the whole system.

with A_i, $K_{u,i}$, D_i being respectively the intra-sublattice exchange constants, the magnetic uniaxial anisotropy constants, and the anisotropic exchange constants. The magnetostatic interactions $\epsilon_{dmg,i}$ are accounted for by means of two terms: $K_{dmg,i}$ and $K_{sh,i}$, the former entering in the computation of the DW width Δ, and the latter determining the DW type, either Bloch or Néel type. Due to the low net magnetization of the system, these terms can be considered as negligible if compared with the uniaxial anisotropy and the anisotropic exchange terms, but they are here included for the sake of a more general treatment of the system. Finally, (H_x, H_y, H_z) are the vector components of any external field $\vec{H}_{ext}$. In addition to these terms, and inter-sublattice exchange interaction

must be considered, which is postulated to be in the form:

$$\epsilon_{12} = -B_{12}\vec{m}_1 \cdot \vec{m}_2 = -B_{12}\sin\theta_1 \sin\theta_2 \cos\left(\phi_1 - \phi_2\right) + \cos\theta_1 \cos\theta_2, \quad \text{(A.2)}$$

where the constant B_{12} determines that the interaction promotes antiparallel (parallel) alignment of the sublattices if $B_{12} > 0$ ($B_{12} < 0$). Field-like spin-orbit torque (FL-SOT) can also be included at this point, and is written as:

$$\epsilon_{SOT,i} = -\mu_0 M_{s,i} H_{FL,i} \vec{\sigma} \cdot \vec{m}_i, \quad \text{(A.3)}$$

where $\vec{\sigma} = \vec{u}_J \times \vec{u}_z = -\vec{u}_y$, for a longitudinal current so that $\vec{u}_J = \vec{u}_x$,[18, 15, 19] and $H_{FL,i}$ represents the amplitude of the FL-SOT. Each term is to be added to the respective sublattice.

The use of the mentioned ansatz results in the following identities:

$$\nabla\theta_i = \frac{\partial\theta_i}{\partial x} = +Q_i \frac{\sin\theta_i}{\Delta} \quad , \qquad \nabla\phi_i = \nabla\psi_i = 0, \quad \text{(A.4a)}$$

$$\delta\theta_i = -Q_i \frac{\sin\theta_i}{\Delta}\delta q \quad , \qquad \delta\phi_i = \delta\psi_i = 0, \quad \text{(A.4b)}$$

$$\dot{\theta}_i = -Q_i \frac{\sin\theta_i}{\Delta}\dot{q} \quad , \qquad \dot{\phi}_i = \dot{\psi}_i. \quad \text{(A.4c)}$$

Once all energy density terms have been established, they can be integrated along the longitudinal direction to obtain the total areal energy density σ of the system as $\sigma = \int_{-\infty}^{+\infty} \left(\epsilon_1 + \epsilon_2 + \epsilon_{12}\right) dx$, resulting in the value:

$$\begin{aligned}
\sigma = {} & \frac{2A_1}{\Delta} + 2\Delta\left(K_{eff,1} + K_{sh,1}\sin^2\psi_1\right) + \pi\ Q_1 D_1 \cos\psi_1 - \\
& - \mu_0 M_{s,i}\pi\Delta\left(H_x\cos\psi_1 + H_y\sin\psi_1\right) - 2Q_1\mu_0 M_{s,1} q H_z + \\
& + \frac{2A_2}{\Delta} + 2\Delta\left(K_{eff,2} + K_{sh,2}\sin^2\psi_2\right) + \pi\ Q_2 D_2 \cos\psi_2 - \\
& - \mu_0 M_{s,2}\pi\Delta\left(H_x\cos\psi_2 + H_y\sin\psi_2\right) - 2Q_2\mu_0 M_{s,2} q H_z - \\
& - 2B_{12}\Delta\cos\left(\psi_2 - \psi_1\right) + \mu_0\pi\Delta\left(M_{s,1}H_{FL,1}\sin\psi_1 + M_{s,2}H_{FL,2}\sin\psi_2\right).
\end{aligned} \quad \text{(A.5)}$$

This expression has been obtained by using the following intermediate identities: $\int_{-\infty}^{+\infty}\sin\theta_i dx = \pi\Delta$, $\int_{-\infty}^{+\infty}\sin^2\theta_i dx = 2\Delta$, and $\int_{-\infty}^{+\infty}\cos\theta_i dx = 2Q_i q$.

Additionally to the areal energy term, the kinetic K_i and dissipation F_i terms per unit area for each sublattice are also worked out by integrating along the longitudinal axis their respective expressions:

$$K_i = \int_{-\infty}^{+\infty} \left[\frac{\mu_0 M_{s,i}}{\gamma_i} \phi_i \sin\theta_i \dot{\theta}_i - \frac{\mu_0 M_{s,i}}{\gamma_i} \phi_i \sin\theta_i \left(u_i \vec{u}_J \cdot \nabla \right) \theta_i \right] dx = \\ = -2Q_i \frac{\mu_0 M_{s,i}}{\gamma_i} \left(\dot{q} + u_i \right) \psi_i, \tag{A.6a}$$

$$F_i = \int_{-\infty}^{+\infty} \frac{\alpha_i \mu_0 M_{s,i}}{\gamma_i} \left\{ \left[\frac{d}{dt} - \frac{\beta_i}{\alpha_i} \left(u_i \vec{u}_J \right) \right] \vec{m}_i - \frac{\gamma_i}{\alpha_i} H_{SL,i} \vec{m}_i \times \vec{\sigma} \right\}^2 dx = \\ = \frac{\alpha_i \mu_0 M_{s,i}}{\gamma_i} \Delta \left[\frac{\dot{q}^2}{\Delta^2} + \dot{\psi}_i^2 \right] + \frac{\mu_0 M_{s,i}}{\gamma_i} 2\beta_i u_i \frac{\dot{q}}{\Delta} + Q_i \mu_0 \pi M_{s,i} H_{SL,i} \dot{q}, \tag{A.6b}$$

It is to note that only the relevant terms are written down in the expression of the dissipation term, i.e., those depending on $\dot{q}$ or $\dot{\psi}_i$. These expressions include the adiabatic spin transfer torques, given by some u_i values,[26] their non-adiabatic counterparts, related to the latter by the β_i parameters, and the Slonczewski-like terms of the spin-orbit torques (SL-SOT), accounted for by the $H_{SL,i}$ factors, as they have been defined in the main text. Together with the previously presented intermediate results, the following ones must be considered in this calculation: $\int_{-\infty}^{+\infty} \sin\theta_i \dot{\theta}_i dx = -2Q_i \dot{q}_i$, and $\int_{-\infty}^{+\infty} \dot{\theta}_i^2 dx = \frac{q_i^2}{\Delta} + \Delta \dot{\psi}_i^2$.

Dynamic equations can be derived by building up the lagrangian $L = \sigma + K$, with $K = K_1 + K_2$, and the dissipation function $F = F_1 + F_2$, and applying the Euler-Lagrange-Rayleigh conditions $\frac{\partial L}{\partial X} - \frac{d}{dt}\left(\frac{\partial L}{\partial \dot{X}}\right) + \frac{\partial F}{\partial \dot{X}} = 0$, with $X = \{q, \psi_1, \psi_2\}$,[26] resulting in the set of equations presented in the main text.

References

[1] Stuart S. P. Parkin, Masamitsu Hayashi, and Luc Thomas. Magnetic domain wall racetrack memory. *Science*, 320:190, 2008.

[2] Kab-Jin Kim, Jae-Chul Lee, Sang-Jun Yun, Gi-Hong Gim, Kang-Soo Lee, Sug-Bong Choe, and Kyung-Ho Shin. Electric control of multiple domain walls in pt/co/pt nanotracks with perpendicular magnetic anisotropy. *Applied Physics Express*, 3:083001, 2010.

[3] A. Thiaville, S. Rohart, E. Jue, V. Cros, and A. Fert. Dynamics of dzyaloshinskii domain walls in ultrathin magnetic films. *Europhysics Letters*, 100:57002, 2012.

[4] G. Chen, J. Zhu, A. Quesada, J. Li, A. T. N'Diaye Y. Huo, T. P. Ma, Y. Chen, H.Y. Kwon, C. Won, Z. Q. Qiu, A. K. Schmid, and Y. Z. Wu. *Physical Review Letters*, 110:177204, 2013.

[5] J.-P. Tetienne, T. Hingant, L.J. Martínez, S. Rohart, A. Thiaville, L. Herrera Diez, K. Garcia, J.-P. Adam, J.-V. Kim, J.-F. Roch, I.M. Miron, G. Gaudin, L. Vila, B. Ocker, D. Ravelosona, and V. Jacques. The nature

of domain walls in ultrathin ferromagnets revealed by scanning nanomagnetometry. *Nature Communications*, 6:6733, 2015.

[6] A. Mougin, M. Cormier, J. P. Adam, P. J. Metaxas, and J. Ferré. Domain wall mobility, stability and walker breakdown in magnetic nanowires. *Europhysics Letters*, 5:57007, 2007.

[7] Eduardo Martinez. Static properties and current-driven dynamics of domain walls in perpendicular magnetocrystalline anisotropy nanostrips with rectangular cross-section. *Advances in Condensed Matter Physics*, 2012:954196, 2012.

[8] Eduardo Martinez, Satoru Emori, Noel Perez, Luis Torres, and Geoffrey S. D. Beach. Current-driven dynamics of dzyaloshinskii domain walls in the presence of in-plane fields: Full micromagnetic and one-dimensional analysis. *Journal of Applied Physics*, 115:213909, 2014.

[9] C. Garg, S.-H. Yang, T. Phung, A. Pushp, and S. S. P. Parkin. Dramatic influence of curvature of nanowire on chiral domain wall velocity. *Science Advances*, 3, 2017.

[10] Robin Bläsing, Tianping Ma, See-Hun Yang, Chirag Garg, Fasil Kidane Dejene, Alpha T N'Diaye, Gong Chen, Kai Liu, and Stuart S. P. Parkin. Exchange coupling torque in ferrimagnetic co/gd bilayer maximized near angular momentum compensation temperature. *Nature Communications*, 9:4984, 2018.

[11] Óscar Alejos, Víctor Raposo, Luis Sanchez-Tejerina, Riccardo Tomasello, Giovanni Finocchio, and Eduardo Martinez. Current-driven domain wall dynamics in ferromagnetic layers synthetically exchange-coupled by a spacer: A micromagnetic study. *Journal of Applied Physics*, 123(1):013901, 2018.

[12] Lucas Caretta, Maxwell Mann, Felix Büttner, Kohei Ueda, Bastian Pfau, Christian M. Günther, Piet Hessing, Alexandra Churikova, Christopher Klose, Michael Schneider, Dieter Engel, Colin Marcus, David Bono, Kai Bagschik, Stefan Eisebitt, and Geoffrey S. D. Beach. Fast current-driven domain walls and small skyrmions in a compensated ferrimagnet. *Nature Nanotechnology*, 3, 2018.

[13] Soong-Geun Je, Juan-Carlos Rojas-Sánchez, Thai Ha Pham, Pierre Vallobra, Gregory Malinowski, Daniel Lacour, Thibaud Fache, Marie-Claire Cyrille, Dae-Yun Kim, Sug-Bong Choe, Mohamed Belmeguenai, Michel Hehn, Stéphane Mangin, Gilles Gaudin, and Olivier Boulle. Spin-orbit torque-induced switching in ferrimagnetic alloys: Experiments and modeling. *Applied Physics Letters*, 112:062401, 2018.

[14] Duck-Ho Kim, Takaya Okuno, Se Kwon Kim, Se-Hyeok Oh, Tomoe Nishimura, Yuushou Hirata, Yasuhiro Futakawa, Hiroki Yoshikawa, Arata

Tsukamoto, Yaroslav Tserkovnyak, Yoichi Shiota, Takahiro Moriyama, Kab-Jin Kim, Kyung-Jin Lee, and Teruo Ono. Low magnetic damping of ferrimagnetic gdfeco alloys. *Physical Review Letters*, 122:127203, 2019.

[15] P. P. J. Haazen, E. Mure, J. H. Franken, R. Lavrijsen, H. J. M. Swagten, and B. Koopmans. *Nature Materials*, 12:299, 2013.

[16] S. Zhang and Z. Li. *Physical Review Letters*, 93:1, 2004.

[17] Chung T. Ma, Xiaopu Li, and S. Joseph Poon. Micromagnetic simulation of ferrimagnetic tbfeco films with exchange coupled nanophases. *Journal of Magnetism and Magnetic Materials*, 417:197–202, 2016.

[18] Kwang-Su Ryu, Luc Thomas, See-Hun Yang, and Stuart Parkin. *Nature Nanotechnology*, 8:527–533, 2013.

[19] Satoru Emori, Uwe Bauer, Sung-Min Ahn, Eduardo Martínez, and Geoffrey S. D. Beach. *Nature Materials*, 12:611–616, 2013.

[20] E. Martínez, S. Emori, and G. S. D. Beach. *Applied Physics Letters*, 103:072406, 2013.

[21] J. Vogel, M. Bonfim, N. Rougemaille, O. Boulle, M. Miron, S. Auffret, B. Rodmacq, G. Gaudin, J. C. Cezar, F. Sirotti, and S. Pizzini. Direct observation of massless domain wall dynamics in nanostripes with perpendicular magnetic anisotropy. *Physical Review Letters*, 108:247202, 2012.

[22] Jacob Torrejon, Eduardo Martínez, and Masamitsu Hayashi. Tunable inertia of chiral magnetic domain walls. *Nature Communications*, 7:13533, 2016.

[23] Jonas Seib and Manfred Fähnle. Calculation of the gilbert damping matrix at low scattering rates in gd. *Physical Review B*, 82(6):064401, 2010.

[24] Bernard Diény. Giant magnetoresistance in spin-valve multilayers. *Journal of Magnetism and Magnetic Materials*, 136:335–359, 1994.

[25] Xin Jiang, Li Gao, Jonathan Z. Sun, and Stuart S. P. Parkin. Temperature dependence of current-induced magnetization switching in spin valves with a ferrimagnetic cogd free layer. *Physical Review Letters*, 97:217202, 2006.

[26] A. Thiaville, Y. Nakatani, J. Miltat, and N. Vernier. *Journal of Applied Physics*, 95(11):7049, 2004.